J Solid State Electrochem (2000) 4: 189–198

ORIGINAL PAPER

Mandira Madhuchhanda · Nihar B. Devi
K. Srinivasa Rao · P.C. Rath · R.K. Paramguru

Galvanic interaction between sulfide minerals and pyrolusite

Received: 22 February 1999 / Accepted: 17 August 1999

Abstract Galvanic interaction between manganese dioxide and sulfide mineral (FeS_2, $CuFeS_2$, ZnS and PbS) galvanic couples were investigated through polarization measurements and leaching studies. The sulfide minerals, being less noble than MnO_2, form the anode in each couple, with MnO_2 the cathode. Both sulfide minerals and MnO_2 dissolve at an enhanced rate under the influence of the potential difference between the electrodes of the couple acting as the driving force. Polarization studies provided information on the individual half-cell reactions as well as the galvanic interactions. The kinetics and mechanism of the performance of these galvanic couples were examined by applying electrochemical principles. Hydrogen ions were found to have a prominent effect on the galvanic current observed for the MnO_2-FeS_2 and MnO_2-$CuFeS_2$ couples, which was less for the MnO_2-ZnS couple and became totally ineffective in the case of the MnO_2-PbS couple. The interaction occurred in the Tafel regions of each of the half-cell reactions of the first three couples, whereas it occurred in the Tafel-limiting current regions of the last couple. The cathodic reduction of MnO_2 was found to be slower and rate controlling in the case of the MnO_2-FeS_2 couple, whereas the diffusion-controlled anodic oxidation of galena was rate controlling for the MnO_2-PbS couple. The other two couples were under mixed control. These trends in the mode of operation of these four galvanic couples were as per the change in the noble character of the four sulfide minerals. The effect of the solid/liquid ratio and the sulfide/MnO_2 ratio on the galvanic interaction during particulate leaching was also investigated.

M. Madhuchhanda · N.B. Devi · K. Srinivasa Rao
P.C. Rath · R.K. Paramguru (✉)
Hydro & Electrometallurgy Division,
Regional Research Laboratory,
Council of Scientific & Industrial Research,
Bhubaneswar 751013, Orissa, India
e-mail: root@csrrlbhu.ren.nic.in

Key words Sulfide mineral · Manganese dioxide · Galvanic interaction · Mixed potential · Polarization

Introduction

Galvanic interaction between semiconducting sulfide-sulfide minerals has been reported in the literature for a long time. It plays a significant role in hydrometallurgical operations like wet grinding [1, 2], flotation [3–5] and leaching [6–10]. However, reports about sulfide-pyrolusite galvanic interaction are only recent [11–13]. Here, both the minerals of the galvanic couple corrode (MnO_2 as the cathode and the sulfide mineral as the anode). The probable reactions representing such systems may be written as:

Anodic:

$$MeS_x \rightleftharpoons Me^{2+} + xS + 2e^- \quad (1)$$

$$MeS_x + 4xH_2O \rightleftharpoons Me^{2+} + xSO_4^{2-} + 8xH^+ + (2 + 6x)e^- \quad (2)$$

Cathodic:

$$MnO_2 + 4H^+ + 2e^- \rightarrow Mn^{2+} + 2H_2O \quad (3)$$

It has also been reported that a combination of polarization measurements and leaching tests not only enables quantitative determination of galvanic interaction, but also allows evaluation of the mechanism of the process [13]. In the case of the FeS_2-MnO_2 [13] and ZnS-MnO_2 [12] couples, the open circuit dissolution rates in 0.1 M H_2SO_4 were found to be of the order of 0.24, 0.09 and 0.03 mA/cm^2 for MnO_2, FeS_2 and ZnS, respectively, whereas the galvanic currents resulting from the FeS_2-MnO_2 and ZnS-MnO_2 contacts were 1.75 and 2.45 mA/cm^2, respectively. This means that galvanic interaction in these cases is highly significant in comparison to their self-corrosion phenomena. This may be

due to the large gap between the rest potentials of ZnS/FeS_2 and that of MnO_2. These results suggest that there is tremendous scope for exploiting galvanic interaction, on a commercial scale, to effectively leach out sulfide and MnO_2 ore bodies with a large particulate surface area. It may be mentioned that chalcopyrite, sphalerite and galena ores/concentrates are the commercial source of copper, zinc and lead, respectively. These minerals do not dissolve easily in dilute mineral acids in the absence of an oxidant, or the pyrolusite ore (MnO_2) in the absence of a reducing agent. Hence, a roasting step is employed in the treatment of these ore bodies in order to make them amenable for easy processing. Thus, successful application of galvanic interaction during particulate leaching of a MS-MnO_2 system is likely to provide an attractive alternative for commercial exploitation of these ores. Further, it may open up a new vista of electroregenerative leaching in the area of extractive metallurgy.

The concepts already developed in the field of metal corrosion are applicable to the electronically conducting solids immersed in electrolytes where coupled interfacial charge-transfer takes place. A simple and reliable approach to study such systems is to analyze Evans diagrams obtained by superimposition of the polarization curves of the individual half-cell reactions. This allows one to determine the galvanic potential, E_g, and the galvanic current, i_g. Further, the position of E_g with respect to the region of the particular half-cell polarization plot guides one to derive rate expressions for the galvanic interaction. Wadsworth [14] derived rate equations for mixed potential galvanic couples. Nowak et al. [15] and Holmes and Crundwell [16] have also attempted to derive mathematical models which describe the magnitude of the galvanic interaction in terms of thermodynamic and kinetic parameters. The Butler-Volmer equation, which describes the relationship between the rate of an electrochemical reaction and its thermodynamic and kinetic parameters, was used to quantify the magnitude of the galvanic interaction between minerals. While these authors [14–16] have dealt with galvanic interaction between either sulfide-sulfide mineral couples or sulfide mineral-metal couples, others [11–13] have examined sulfide (sphalerite and pyrite) mineral-pyrolusite couples.

With this background information, the present work is an attempt to examine further details of the galvanic interaction for four couples, namely pyrite-pyrolusite, chalcopyrite-pyrolusite, sphalerite-pyrolusite and galena-pyrolusite. The specific objective is to look for details about the individual half-cell reactions of each of these couples that would lead to a better understanding of the kinetics and mechanism of the galvanic interaction. The effects of specific parameters such as potential difference, temperature, electrolyte concentrations and level of galvanic contact during particulate leaching have been examined. Both polarization measurements and some leaching studies in sulfate and chloride media have been employed to make the study.

Experimental

Materials

Pyrolusite

A pyrolusite sample (manganese dioxide ore) collected from Nishikhal deposits of Orissa, India, containing 58.41% MnO_2, 2.55% Mn_2O_3, 0.13% MnO, 17.34% Fe_2O_3, 8.00% Al_2O_3, 9.72% SiO_2, 1.73% CaO, 0.57% MgO, 0.42% K_2O and 0.10% Na_2O was powdered and used for leaching studies. The X-ray diffraction pattern of the ore sample revealed that pyrolusite is the major mineral and α-quartz, cryptomelane and goethite are present in minor quantities. For electrode preparation, synthetically prepared β-MnO_2, containing 62.11% Mn^{4+}, 0.29% Mn^{3+}, 0.04% Mn^{2+} and 0.59% H_2O, was used. The diffraction pattern of this sample shows characteristics of β-MnO_2 or the mineral pyrolusite.

Pyrite

A pyrite sample was collected from the Amjhor pyrite deposit of Bihar, India. The grade of the sample conformed to 42.76% Fe, 47.88% S, 6.39% SiO_2, 0.37% Mg, 0.51% Ca, 0.13% Na and 0.15% K. The X-ray diffraction pattern of this sample showed pyrite as the major mineral and one weak peak of α-quartz as the impurity. The FeS_2 content of the sample was estimated to be 89.78%. The sample was powdered and used for electrode preparation and leaching studies.

Chalcopyrite

Chalcopyrite concentrate was obtained from Hindustan Copper, Ghatsila (Rakha mines), Bihar, India. The chemical analysis showed 21.0% Cu, 35.2% Fe, 32.5% S and 8.6% acid insolubles. The X-ray diffraction pattern showed chalcopyrite as the only copper mineral and pyrite as the major impurity.

Sphalerite

Sphalerite concentrate was obtained from Rajpura Dariba Mills of Hindustan Zinc, Udaipur, Rajasthan, India, and its grade was 53.00% Zn, 1.80% Pb, 5.65% Fe, 0.20% Cu, 37.00% S and 2.40% acid insolubles. The X-ray diffraction pattern indicated sphalerite and pyrite as the major minerals.

Galena

High pure galena lumps were hand picked from the Saintala area of Bolangir district in Orissa, India. The chemical analysis of the sample showed 84.30% Pb, 12.93% S and 2.58% SiO_2. The X-ray diffraction pattern confirmed galena as the major mineral.

All the materials were ground to −100 BSS mesh size before use.

Preparation of electrodes

Five grams of the powdered ore sample were mixed thoroughly with 1 g graphite and 1 g (0.5 g in case of MnO_2) of transoptic powder (Buehler, USA) (the former was added to increase the conductivity whereas the latter was used as a binder). The mixture was then compacted in a cylindrical stainless steel mould of 2.5 cm diameter (Simplement II, Buehler, USA) under a pressure of 0.34 kbar at 130 ± 5 °C for 30 min. A conducting wire was attached to one side of the compressed pellet with the help of a silver-based conducting cement and the pellet was mounted in an epoxy resin, embedding the surface in contact with the conducting

wire. The exposed geometric surface area of the electrode was 5 cm^2.

Polarization measurements

Polarization measurements were made using a conventional three-electrode cell as described in earlier publications [9, 13]. One of the sulfide minerals or MnO_2 was the working electrode, whereas platinum and a saturated calomel electrode (SCE) were used as counter and reference electrodes, respectively. Polarization curves were plotted using a Model 362 Scanning Potentiostat (EG&G) coupled with a series 2000 Omnigraphic X-Y recorder (Houston Instruments). All potentials recorded in this study were against the SCE.

Leaching studies

Leaching studies on powder samples were carried out in a glass reactor immersed in a water bath. The reactor was fitted with a thermometer, condenser, stirrer and an opening for charging and withdrawal of the sample. The water bath was heated to maintain the required temperature within ± 1 °C. The required amount of leachant was taken in the reactor and heated. The material was charged at desirable temperatures and the reaction was initiated. Aliquots were drawn at regular intervals and analyzed by atomic absorption spectrophotometry. Ferrous ion was determined by a standard classical method and pH was measured using a pH meter.

Distilled water and reagent grade acids were used to make the solutions.

Results and discussion

Figures 1 and 2 show superposition of individual galvanostatic anodic polarization curves for FeS_2, $CuFeS_2$, ZnS and PbS electrodes against the cathodic plot of the MnO_2 electrode in 0.1 M HCl and H_2SO_4 electrolytes, respectively. The PbS electrode was not used in H_2SO_4 medium because it is known that $PbSO_4$ formed on the surface is insoluble in this medium. In HCl media, 1.0 M NaCl was added in the case of PbS in order to increase the solubility of the $PbCl_2$ product. These curves represent the following reactions:

Anodic:

$$\text{Pyrite}\quad FeS_2 + 4H_2O \rightarrow Fe^{2+} + 2SO_4^{2-} + 16H^+ + 14e^- \tag{4}$$

$$\text{Chalcopyrite}\quad CuFeS_2 \rightarrow Cu^{2+} + Fe^{2+} + 2S^0 + 4e^- \tag{5}$$

$$\text{Sphalerite}\quad ZnS \rightarrow Zn^{2+} + S^0 + 2e^- \tag{6}$$

$$\text{Galena}\quad PbS \rightarrow Pb^{2+} + S^0 + 2e^- \tag{7}$$

Cathodic:

$$\text{Pyrolusite}\quad MnO_2 + 4H^+ + 2e^- \rightarrow Mn^{2+} + 2H_2O \tag{8}$$

Coulumbic efficiencies determined from analysis of the solution, in which the MS-MnO_2 electrode couples were kept suspended for a prolonged period under electrical contact, revealed that reaction 8 is the sole cathodic contributor in the case of all four couples. Reactions 4 and 7 are the anodic contributors for the FeS_2-MnO_2 and PbS-MnO_2 couples, respectively. In the case of $CuFeS_2$-MnO_2 and ZnS-MnO_2 couples, a combination of reaction 4 with reactions 5 and 6, respectively, corresponded to the total anodic current. This is because of the FeS_2 impurity present in these two electrodes.

Some other salient observations are described in the following sections.

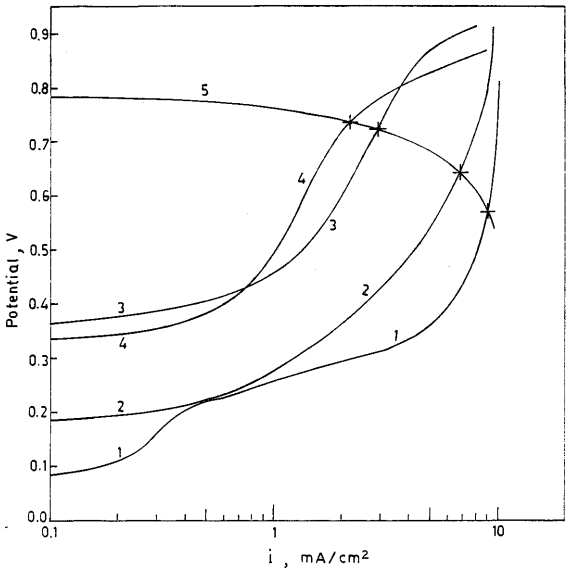

Fig. 1 Concurrent anodic polarization curves of PbS (*1*), ZnS (*2*), $CuFeS_2$ (*3*) and FeS_2 (*4*) against a cathodic plot of MnO_2 (*5*) in 0.1 M HCl at room temperature. Ramp rate: 1 mA/s. 1 M NaCl incorporated in the bath in case of the PbS electrode

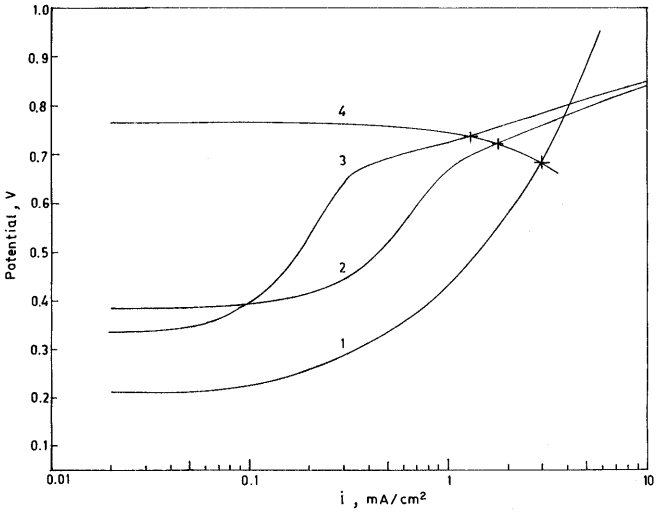

Fig. 2 Concurrent anodic polarization curves of ZnS (*1*), $CuFeS_2$ (*2*) and FeS_2 (*3*) against a cathodic plot of MnO_2 (*4*) in 0.1 M H_2SO_4 at room temperature. Ramp rate: 1 mA/s

Rest potentials

All five electrodes took some time before giving stable rest potentials and approximately 2 h were allowed for

this purpose. The rest potentials of the individual electrodes in H_2SO_4 and HCl electrolytes did not differ significantly (Table 1). The rest potentials of the sulfide electrodes increased in the order galena-sphalerite-pyrite-chalcopyrite, suggesting their noble character in the same order. With respect to the open circuit potential, pyrite is reported to be the most noble mineral amongst these four (column 5, Table 1) [3, 17]. In this case, the presence of pyrite as impurity in the chalcopyrite sample might have resulted in a higher rest potential. However, polarization curves for pyrite, both in H_2SO_4 and HCl media, fall above the plot for chalcopyrite, which indicates that pyrite behaves as the noblest amongst the four. The Nernst relationship for these five electrodes corresponding to reactions 4–8 may be represented as follows:

$$E_{FeS_2} = E^{\circ}_{FeS_2} + (2.303RT/14F)\log\left\{[Fe^{2+}][SO_4^{2-}]^2[H^+]^{16}\right\} \quad (9)$$

$$E_{CuFeS_2} = E^{\circ}_{CuFeS_2} + (2.303RT/4F)\log\{[Cu^{2+}][Fe^{2+}]\} \quad (10)$$

$$E_{ZnS} = E^{\circ}_{ZnS} + (2.303RT/2F)\log\{[Zn^{2+}]\} \quad (11)$$

$$E_{PbS} = E^{\circ}_{PbS} + (2.303RT/2F)\log\{[Pb^{2+}]\} \quad (12)$$

$$E_{MnO_2} = E^{\circ}_{MnO_2} + (2.303RT/2F)\log\left\{[H^+]^4/[Mn^{2+}]\right\} \quad (13)$$

Here, R,T and F are, respectively, the universal gas constant, absolute temperature and Faraday's constant; E° is the standard equilibrium potential of the respective electrodes.

The values reported in the literature for the rest potential E [3, 17] and E° [18–21] for sulfide electrodes are presented in Table 1 along with the E values measured in this study. They compare reasonably well. The E° values should equal the E values at standard electrolyte conditions. However, in some of the cases, specifically for FeS_2 and $CuFeS_2$, these values differ considerably (Table 1). In these cases the reaction is complex because of the formation of a number of intermediate products and in practice a number of reactions occur simultaneously and the value of E is the resultant of all these reactions, whereas E° is evaluated based on a single reaction.

Equations 9–13 indicate that the rest potential of each of the mineral electrodes would be influenced when its own component metal ions are present in the bath. Hydrogen ions in the electrolyte should influence only two of the electrodes, namely FeS_2 and MnO_2. Rest potentials were determined experimentally at three different acid concentrations for these five electrodes, out of which the $CuFeS_2$, ZnS and PbS electrodes were found insensitive towards variation in hydrogen ion concentration. The changes of rest potential with varying hydrogen ion concentrations for MnO_2 and FeS_2 electrodes are shown in Fig. 3. The rest potential of the MnO_2 electrode in both H_2SO_4 and HCl electrolytes increases at a rate of 0.145 V per decade of $[H^+]$, which may be considered close to the value of 0.118 V per decade (at 298 K) predicted from Eq. 13. As far as E_{FeS2} is concerned, the value of 0.036 V per decade in HCl and 0.027 V per decade in H_2SO_4 media do not match with 0.067 V per decade (at 298 K) predicted from Eq. 9. Previously, Wei and Osseo-Asare [22] and Lowson [18] have reported a linear variation of the open-circuit potential of FeS_2 on pH, following the Nernst relationship. Whereas the former, using synthetic FeS_2, observed this for the entire pH range, the latter observed the relationship only in the pH range 2–12, the potential becoming independent of $[H^+]$ below a pH value of 2. Since the pH is below 1 in the present case, the rest potential did not obey the exact Nernst relationship. However, there is a trend of a linear dependence of E_{FeS2} on $[H^+]$.

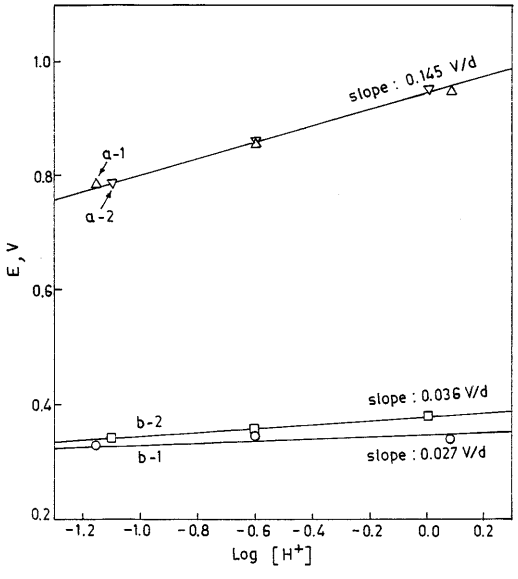

Fig. 3 Potential versus log$[H^+]$ plots: *a* rest potential of MnO_2 electrode; *b* rest potential of FeS_2 electrode; *1* H_2SO_4; *2* HCl

Table 1 Rest potential E (SCE) of different electrodes used in this study in acidic electrolyte

Serial no.	Mineral present	Reaction no.	E (V) this study[a]	E (V) [3, 17]	E° (V) [18–21]
1	FeS_2	4	0.34 (0.33)	0.42	0.14
2	$CuFeS_2$	5	0.36 (0.38)	0.32	0.17
3	ZnS	6	0.19 (0.20)	0.22	0.06
4	PbS	7	0.08	0.16	0.11
5	MnO_2	8	0.95 (0.94)	–	0.99

[a] In 0.1 M HCl. Bracketed values in 0.1 M H_2SO_4

Shape of the polarization curves

The polarization plots for each electrode are similar in both Figs. 1 and 2, indicating identical processes in H_2SO_4 and HCl electrolytes. The anodic plots for FeS_2 in both electrolytes show a small passivating region, which may be due to some adsorbed species [11, 13, 23]. However, a linear portion, which may be termed as the transpassive Tafel region, prevails subsequently. The slope of this region is ~0.130 V per decade. It may be mentioned that the passivating region does not appear in the reverse sweep. The anodic plots for chalcopyrite are identical to that of pyrite, showing a small passivating region up to around 0.8 V, beyond which a transpassive Tafel region occurs with a slope of 0.160 V per decade. Such a passive-like response during anodic polarization of chalcopyrite has also been reported before [24, 25] and it was thought to be due to the formation of a surface film consisting of metal-deficient polysulfides. The anodic plot for galena, obtained only in chloride medium, shows clear-cut Tafel and limiting current regions. The Tafel slope is 0.120 V per decade, which is close to that observed by other authors [9, 15, 16, 26, 27]. The anodic plot for the ZnS electrode lies between those of chalcopyrite and galena. It does not show either a clear-cut Tafel or a passivating region. It does not show any limiting current region either. This is similar to that observed earlier [28], and may be due to adsorption of a chloro complex covering part of the surface, as suggested by Warren et al. [29]. Starting from an open-circuit potential of 0.784 V, the cathodic polarization plots of MnO_2 electrode in both H_2SO_4 and HCl electrolytes show a much higher corrosion current density in comparison to those of the four sulfide electrodes covered in this study. Hence, one can conclude that the cathodic over-voltage is quite low in comparison to the anodic over-voltage for a definite galvanic current. The cathodic polarization curve for the MnO_2 electrode, however, does not show a clear-cut Tafel region, and may be due to the large corrosion current density for which the effect of concentration polarization becomes significant soon after the Tafel region.

Galvanic interaction between MnO_2 and sulfide minerals

As soon as the electrode pairs, MnO_2-FeS_2, MnO_2-$CuFeS_2$, MnO_2-ZnS or MnO_2-PbS, come in galvanic contact within the electrolyte, the intersection points corresponding to the polarization plots of each pair in Figs. 1 and 2 represent galvanic interaction. The potential corresponding to these points is the galvanic potential, E_g, and the current density is the galvanic current density, i_g. Moreover, the position of this point with respect to a specific region (linear, Tafel or limiting current) of the respective polarization plots determines the mechanism of the process and helps in deriving the rate equations. As mentioned in the previous section, clear-cut Tafel, passivation and/or limiting current regions are recognized in the case of three electrodes, viz. FeS_2, $CuFeS_2$ and PbS, but not in the case of MnO_2 or ZnS. However, the apparent position of the galvanic intersection points may be on the Tafel regions for these two electrodes, as visualized from Figs. 1 and 2. In an earlier work [13], expressions for E_g and i_g have been derived for the MnO_2-FeS_2 galvanic couple, the interaction taking place in the Tafel regions of both the anodic and the cathodic plots. In this situation the Butler-Volmer equation describes the potential-current relation and the derived expressions for E_g and i_g are:

$$E_g = (2.303RT/F)\log K_1[H^+] \tag{14}$$

$$i_g = K_2[H^+]^{1/2} \tag{15}$$

where K_1 and K_2 are constants. The same equations with different constants will be valid for E_g and i_g of the other three galvanic couples if galvanic interaction takes place in the Tafel region of both the plots. When the interaction takes place in the limiting current region of the anodic curve, as in case of the MnO_2-PbS couple, the expression for i_g would not contain the $[H^+]$ term since the anodic reaction 7, which is expected to be rate controlling, does not contain this term and diffusion of $[H^+]$ cannot control the rate. In such a case, the dependence of $\log i_g$ on $\log[H^+]$ would be zero. Figures 4 and 5 present, respectively, the plots of E_g and $\log i_g$ against $\log[H^+]$ using the data obtained from polarization plots at three acid concentrations. The dependence of E_g on $\log[H^+]$ shows higher values than that predicted from Eq. 14 and this value increases in the order FeS_2-$CuFeS_2$-ZnS-PbS. It is worthwhile noting that the position of galvanic interaction shifts from

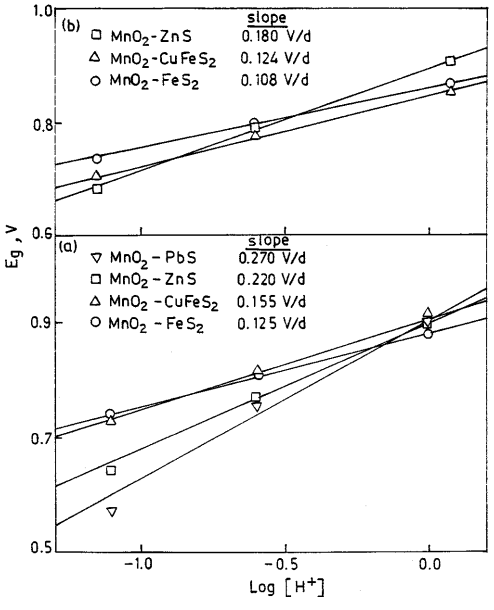

Fig. 4 Galvanic potential versus $\log[H^+]$ plots for MnO_2-MS couples: *a* HCl bath; *b* H_2SO_4 bath. In the case of PbS, 1 M NaCl is incorporated in the bath

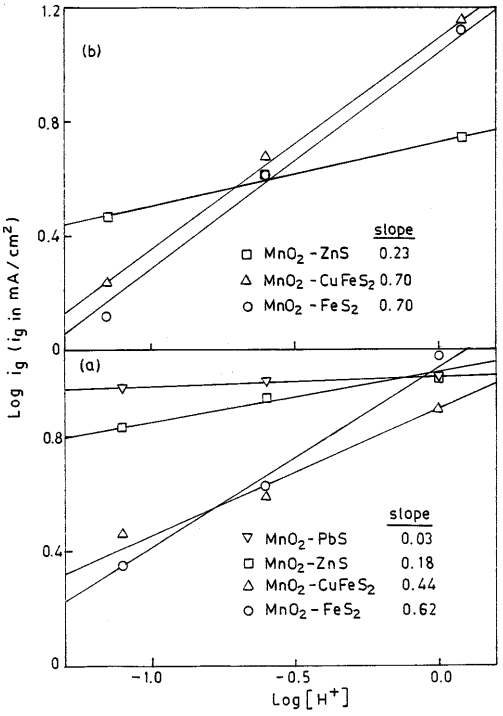

Fig. 5 Logi_g versus log[H^+] plots for MnO_2-MS couples: **a** HCl bath; **b** H_2SO_4 bath. In the case of PbS_2, 1 M NaCl is incorporated in the bath

anodic Tafel to anodic limiting current region in that order. The dependence of logi_g on log[H^+] also shifts in that order, i.e. 0.5 (anodic Tafel) to 0 (anodic limiting current). In case of MnO_2-FeS_2 and MnO_2-$CuFeS_2$ couples, the dependence is closer to 0.5 confirming a Tafel-Tafel interaction as per Eq. 15. For the PbS-MnO_2 couple the dependence is near to zero, a value reasonable for a Tafel-limiting current interaction. For the ZnS-MnO_2 couple, values of 0.18 in HCl and 0.23 in H_2SO_4 media indicate that the interaction is taking place in a region of the anodic plot which is in between the Tafel and limiting current regions. Figures 1 and 2 indeed indicate such a situation for ZnS.

Another important observation is the relative difference of the cathodic (E_c) and the anodic (E_a) rest potentials from E_g (Table 2). In case of all four couples, E_c–E_g is lower than E_g–E_a, indicating that the anodic half-reaction of the galvanic couple has a slower rate and hence is rate controlling.

Temperature dependence

The temperature dependence of the individual half-cell reactions as well as the galvanic interaction can also be determined from this type of study. The rate constant (k) of a chemical reaction, usually related to temperature by the well-known Arrhenius equation, may be replaced by the current density "i" for this purpose in the present cases, provided the electrode potential is unchanged.

Table 2 E_c–E_g and E_g–E_a values observed for the four couples

Serial No.	Mineral couple	E_c–E_g (V)[a]	E_g–E_a (V)[a]
1	MnO_2-FeS_2	0.05 (0.03)	0.40 (0.39)
2	MnO_2-$CuFeS_2$	0.07 (0.04)	0.38 (0.34)
3	MnO_2-ZnS	0.15 (0.08)	0.45 (0.47)
4	MnO_2-PbS	0.22	0.71

[a] Bracketed values refer to sulfuric acid

Since the reversible electrode potential may not be invariant at different temperatures, the temperature kinetic method [27, 30] may be employed. In this method, measurements are carried out with the value of the electrode polarization (overpotential) being kept constant. The resultant activation energy may be termed as the effective activation energy, which can be used to draw important inferences.

Polarization studies were made for each of the electrodes of these four galvanic couples independently at different temperatures and super-positioned couple-wise to derive galvanic current density values. The electrolyte composition of 0.1 M HCl in 1 M NaCl was used for the MnO_2-PbS couple, whereas 0.1 M acid without NaCl was used for the other three couples. Figure 6a–d presents the Arrhenius plots for the couples MnO_2-FeS_2, MnO_2-$CuFeS_2$, MnO_2-ZnS and MnO_2-PbS, respectively. Each figure presents three plots, one using i_g values at different temperatures as the rate, whereas the other two utilize i_c (cathodic) and i_a (anodic) values obtained at selected overpotentials. For the MnO_2-FeS_2 couple the resultant effective activation energy obtained for galvanic interaction using i_g values is 24.4 kJ/mol, whereas those obtained using the cathodic half and anodic processes independently are 20.6 and 9.6 kJ/mol, respectively. The closeness of the effective activation energy value for galvanic interaction to that of the cathodic process indicates that the galvanic interaction process is controlled by the slower cathodic half process. This contradicts the inference drawn in the previous section that, E_g–E_a being greater than E_c–E_g, the process is under anodic control. However, the activation energy values should be accepted as more authentic.

It may also be mentioned that the anodic plots for FeS_2 and $CuFeS_2$ show passivity, which is one reason for the larger E_g–E_a values. Examination of the Tafel-(transpassive Tafel) portions of the MnO_2-FeS_2 and MnO_2-$CuFeS_2$ couples from Fig. 2 indicates that the two half-reaction plots in this portion are apparently symmetrical with respect to the E_g axis, which may result in mixed control. In fact the results of the MnO_2-$CuFeS_2$ couple, though identical to those of the MnO_2-FeS_2 couple, show one difference in that the anodic half-reaction also gives an effective activation energy value of 20.6 kJ/mol, equal to that obtained for the cathodic process, against 24.4 kJ/mol for the galvanic interaction. This shows that it is in a mixed control domain. The effective activation energy values for the MnO_2-ZnS

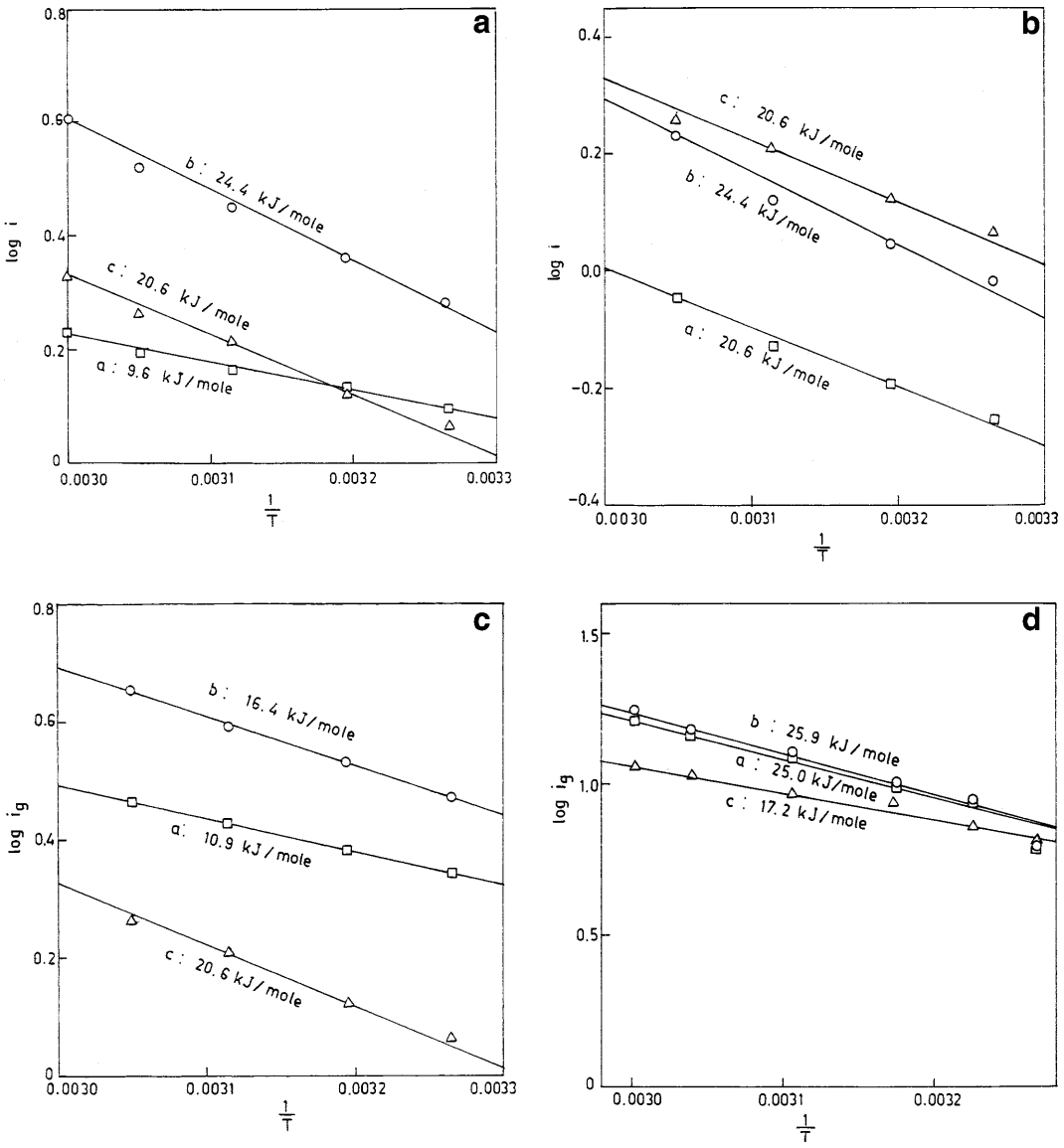

Fig. 6 a Arrhenius plots for MnO_2-FeS_2 couple in 0.1 M H_2SO_4 bath. *a* "*i*" at constant anodic polarization (0.2 V); *b* galvanic current, i_g; and *c* "*i*" at constant cathodic polarization (−0.1 V). **b** Arrhenius plots for MnO_2-$CuFeS_2$ couple in 0.1 M H_2SO_4 bath. *a* "*i*" at constant anodic polarization (0.2 V); *b* galvanic current, i_g; and *c* "*i*" at constant cathodic polarization (−0.1 V). **c** Arrhenius plots for MnO_2-ZnS couple in 0.1 M H_2SO_4 bath. *a* "*i*" at constant anodic polarization (0.4 V); *b* galvanic current, i_g; and *c* "*i*" at constant cathodic polarization (−0.1 V). **d** Arrhenius plots for MnO_2-PbS couple in 0.1 M HCl + 1 M NaCl bath. *a* "*i*" at constant anodic polarization (0.5 V); *b* galvanic current, i_g; and *c* "*i*" at constant cathodic polarization (−0.15 V)

couple are 16.4, 20.6 and 10.9 kJ/mol for galvanic interaction, cathodic and anodic half-processes, respectively. Thus, a further shift towards anodic control is visible, though the process is still in the mixed control region for this couple. The results for galena show activation energy values of 25.9, 25.0 and 17.2 kJ/mol, respectively, for galvanic interaction, anodic and cathodic half-processes. This means that the anodic half-process is slower and controls the interaction. Overall, as the noble character of the sulfide mineral improves, as indicated from the shift of E_a towards a positive direction, the galvanic interaction shifts from anodic to mixed to cathodic control.

Galvanic contact during particulate leaching

The previous sections presented perfect galvanic coupling through external contact of the two planar electrodes. Such contacts may not be possible in hydrometallurgical operations like leaching, which involve suspension of solid particles in a liquid medium. Here galvanic interaction, though an important factor, is effected only through momentary contacts. Such contacts depend on factors like solid-liquid ratio, presence of conducting solids like graphite, agitation, etc. It is therefore necessary to evaluate the effectiveness of the galvanic contact during actual leaching. A limited number of experiments have been reported here to

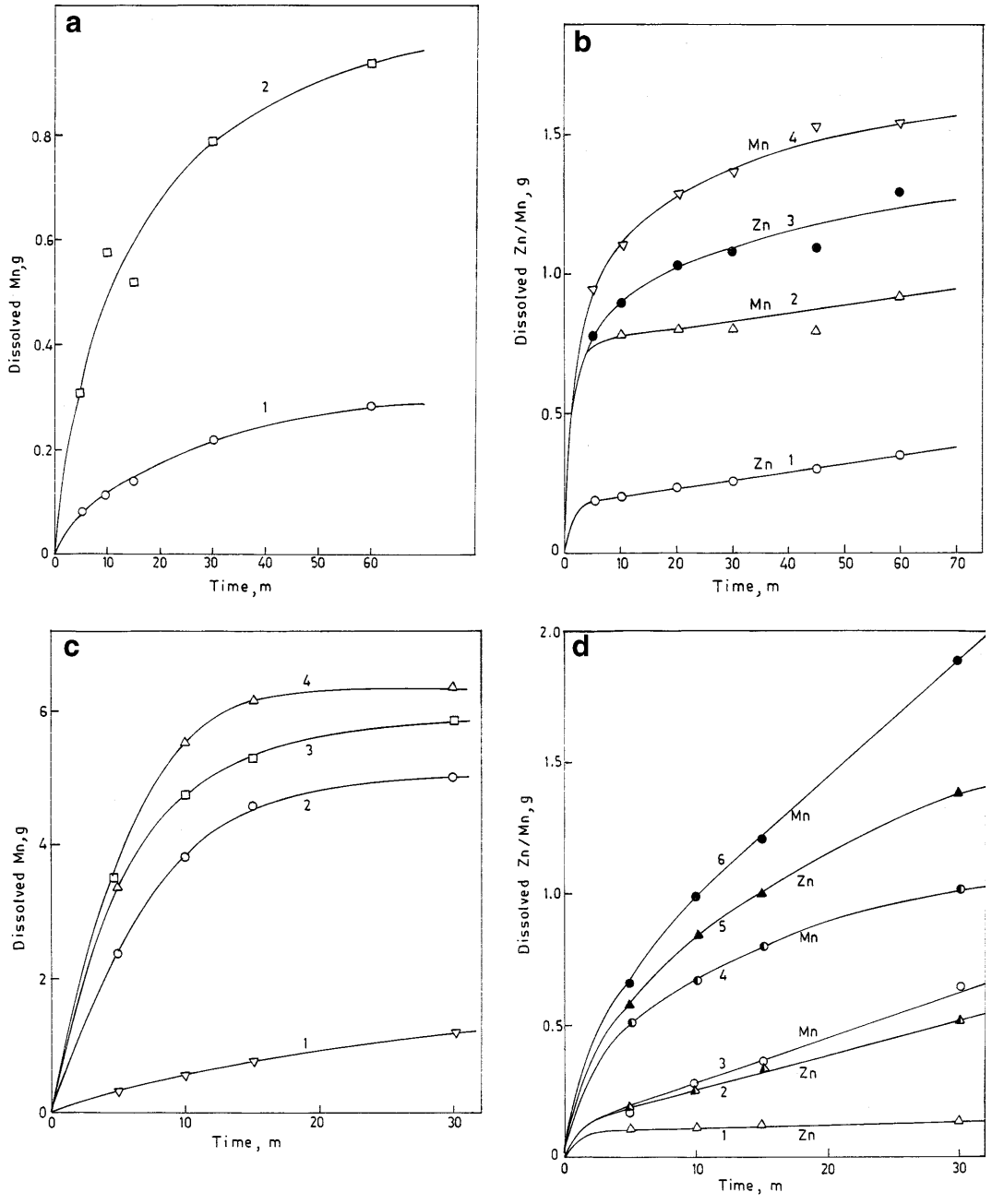

show the effect of the solid-liquid ratio and the proportion of each solid constituent on galvanic contact. Studies were made for MnO_2-$CuFeS_2$ and MnO_2-ZnS couples in H_2SO_4 medium and the results are presented in Fig. 7a and b, respectively. The rates were determined as tangents to the plots between a 5–10 min period and converted to current equivalents using Faraday's law. The surface area was derived from the size and specific gravity of the particles. With 5 g each of chalcopyrite and manganese ore a current equivalent of 0.73 mA/cm^2 for Mn dissolution was obtained which changed to 0.88 mA/cm^2 when 20 g of manganese ore was charged with 5 g of chalcopyrite (Fig. 7a). Similarly, the current equivalent of zinc dissolution improved from 0.24mA/cm^2, when 2 g of sphalerite was leached in presence of 4 g of manganese ore, to 0.36 mA/cm^2 when 10 g each of sphalerite and manganese ore were charged (Fig. 7b). It is clear that galvanic contact is better when the solids concentration in the slurry and the amount of the contacting species are higher. It may be noted that $CuFeS_2$ and ZnS do not dissolve well in this medium when charged independently. However, the presence of MnO_2 effects good dissolution, mainly because of galvanic contact. The fine size of the particles must be providing a large area for galvanic contact.

Particulate leaching studies were also conducted for $CuFeS_2$-MnO_2 and ZnS-MnO_2 couples in HCl medium. In this case, reaction 16 occurs, producing Cl_2 gas which, in turn, also dissolves $CuFeS_2$/ZnS:

◀

Fig. 7 a Dissolution of manganese in the presence of different amount of $CuFeS_2$ in 100 ml 8 M H_2SO_4 at 65 °C. Stirring: 200 rpm. *1* Manganese ore (5 g) + chalcopyrite ore (5 g). *2* Manganese ore (20 g) + chalcopyrite ore (5 g). **b** Dissolution of ZnS and MnO_2 in the presence of each other at different proportions in 100 ml 0.5 M H_2SO_4 containing 0.2 M ferrous sulfate at 60 °C. Stirring: 200 rpm. *1* Plot for Zn with 2 g ZnS + 4 g manganese ore. *2* Plot for Mn with 2 g ZnS + 4 g manganese ore. *3* Plot for Zn with 10 g ZnS + 10 g manganese ore. *4* Plot for Mn with 10 g ZnS + 10 g manganese ore. **c** Dissolution of manganese in the presence of different amounts of chalcopyrite in 100 ml 8 M HCl at room temperature. Stirring: 200 rpm. *1* 20 g manganese ore. *2* 20 g manganese ore + 5 g chalcopyrite. *3* 20 g manganese ore + 10 g chalcopyrite. *4* 20 g manganese ore + 15 g chalcopyrite. **d** Dissolution of ZnS and MnO_2 in the presence of each other at different proportions in 100 ml 4 M HCl at 70 °C. Stirring: 200 rpm. *1* Zn dissolution from 2 g ZnS. *2* Zn dissolution from 2 g ZnS + 5 g MnO_2 ore. *3* Mn dissolution from 2 g ZnS + 5 g MnO_2 ore. *4* Mn dissolution from 6 g ZnS + 5 g MnO_2 ore. *5* Zn dissolution from 6 g ZnS + 15 g MnO_2 ore. *6* Mn dissolution from 6 g ZnS + 15 g MnO_2 ore

$$MnO_2 + 4HCl \rightarrow MnCl_2 + Cl_2 + 2H_2O \qquad (16)$$

Figure 7c and d present the results of these two couples. In these cases, the initial concentration of HCl and the amount of manganese ore were kept constant with a view to maintain the extent of occurrence of reaction 16 constant. However, Fig. 7c and d (plots 3 and 4) show increased dissolution of manganese with increase in $CuFeS_2$ and ZnS content.

Taking the dissolution rates as the tangent to the plots between 5–10 min, the values of the current equivalents of manganese dissolution are 12.23, 15.19 and 17.76 mA/cm^2 at three levels of $CuFeS_2$ in case of $CuFeS_2$-MnO_2 against 1.89 mA/cm^2 in the absence of chalcopyrite (Fig. 7c). The values for zinc dissolution are 2.20 and 4.23 mA/cm^2 at two levels (2 and 5 g of ZnS with 5 g of MnO_2) of ZnS in the case of the ZnS-MnO_2 couple (plots 3 and 4 of Fig. 7d). Plots 5 and 6 in Fig. 7d present the results of manganese and zinc dissolution where the current equivalents were 2.85 and 1.43 mA/cm^2, respectively, when 6 g ZnS and 15 g MnO_2 were leached. With less solid but in the same proportion (2 g ZnS and 5 g MnO_2) the current equivalents for zinc and manganese dissolution were 2.20 and 1.06 mA/cm^2, respectively. The increase in dissolution might have been due to galvanic interaction with a larger surface contact.

The above-mentioned results on particulate leaching suggest that direct leaching of chalcopyrite or sphalerite in dilute mineral acids in the presence of MnO_2 ore may be a practical and viable alternative to roasting. Similarly, manganese ore, for the production of electrolytic manganese dioxide or metal, may be directly leached in the presence of FeS_2 instead of the presently practiced roast-leach method.

Conclusions

The following conclusions may be made from the above-mentioned studies:

1. Polarization studies provide useful data to examine galvanic interaction between MnO_2 and base metal sulfide minerals. Detailed ideas about individual half-cell reactions along with the kinetics and mechanism of galvanic interaction can be derived from such studies.

2. It is known that the noble character of the four sulfide minerals declines in the order pyrite-chalcopyrite-sphalerite-galena. Hence, their potential difference in the galvanic cells with MnO_2 increases in this order. Galvanic interaction between the couples formed by these sulfides with MnO_2 tends from Tafel-Tafel towards Tafel-limiting current regions (cathode-anode) in the same order. In case of MnO_2-FeS_2 and MnO_2-$CuFeS_2$, the interaction occurs in Tafel regions of both the anodic and cathodic half-cell reactions, whereas in the case of MnO_2-PbS it occurs in the Tafel-limiting current regions. MnO_2-ZnS is in-between.

3. This information helps in deriving expressions for E_g and i_g, applying electrochemical principles. The effect of $[H^+]$ was found to be prominent in the case of MnO_2-FeS_2 and MnO_2CuFeS_2 couples, but tended to be insensitive towards MnO_2-ZnS and MnO_2-PbS couples.

4. The cathodic reduction of MnO_2 was found to be slower and rate controlling in the case of the MnO_2-FeS_2 couple, whereas the diffusion-controlled anodic oxidation of galena was rate controlling for the MnO_2-PbS couple. The other two couples were in-between.

Acknowledgements The authors record their gratitude to Prof. H. S. Ray, Director, and Dr. R. P. Das, Deputy Director, Regional Research Laboratory, Bhubaneswar, for their keen interest and permission to publish the paper. The Department of Science and Technology, Government of India, New Delhi, is thanked for supporting this work and the different authorities for providing the mineral samples.

References

1. Natarajan KA, Reimer SC, Iwasaki I (1984) Miner Metall Process 1: 10–14
2. Pozzo RL, Iwasaki I (1987) Miner Metall Process 4: 166–171
3. Majima H (1969) Can Metall Q 8: 269–273
4. Vathsala, Natarajan KA (1989) Int J Miner Process 26: 193–203
5. Yelloji Rao MK, Natarajan KA (1989) Int J Miner Process 27: 279–293
6. Dutrizac JE, MacDonald RJC, Ingraham TR (1971) Can Metall Q 10: 3–7
7. Dutrizac JE, MacDonald RJC (1973) Can Metall Q 12: 409–420
8. Linge HG (1976/77) Hydrometallurgy 2: 219–233
9. Paramguru RK (1992) Met Mater Process 4: 59–76
10. Sarveswara Rao K, Paramguru RK, Das RP, Ray HS (1992) Miner Process Extr Metall Rev 11: 21–37
11. Nayak BB, Parida KM, Rao SB, Sahoo RK, Paramguru RK (1994) Trans Indian Inst Met 47: 27–30
12. Rath PC, Paramguru RK (1994) Met Mater Process 6: 23–30
13. Paramguru RK, Nayak BB (1996) J Electrochem Soc 143: 3987–91
14. Wadsworth ME (1984) Hydromet Proc Fundam 10: 41–76
15. Nowak P, Krauss E, Pomianowski A (1984) Hydrometallurgy 12: 95–110
16. Holmes PR, Crundwell FK (1995) Hydrometallurgy 39: 353–375

17. Yelloji Rao MK, Natarajan KA (1986) Trans Indian Inst Met 39: 582–591
18. Lowson RT (1982) Chem Rev 82: 461–497
19. Mahmood MN, Turner AK (1985) Hydrometallurgy 14: 317–329
20. Garrels RM, Christ CL (1965) Solutions, minerals and equilibria, Harper and Row, New York
21. Miller JD, Wan R (1983) Hydrometallurgy 10: 219–242
22. Wei D, Osseo-Asare K (1996) J Electrochem Soc 143: 3192–3198
23. Peters E, Majima H (1968) Can Metall Q 7: 111–117
24. Parker AJ, Paul RL, Power GP (1981) Aust J Chem 34: 13–34
25. Warren GW, Wadsworth ME, El-Ragby SM (1982) Met Trans 13B: 571–579
26. Paul RL, Nicol MJ, Diggle JW, Saunders AP (1977) Electrochim Acta 23: 625–633
27. Paramguru RK, Ray HS (1996) Min Process Extr Metall Rev 16: 63–87
28. Paramguru RK (1995) Trans Indian Inst Met 48: 295–300
29. Warren GW, Henein H, Jin ZM (1985) Metall Trans 16B: 413–424
30. Antropov LI (1977) Theoretical electrochemistry (Engl. Transl.). Mir, Moscow, pp 335, 418